Fusion Engineering and Design 220 (2025) 115304

Contents lists available at ScienceDirect

Fusion Engineering and Design

journal homepage: www.elsevier.com/locate/fusengdes

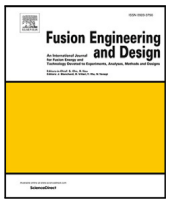

Estimating plasma size by visible emission patterns in the Wendelstein 7-X stellarator

A. Buzás [a,b,*], C. Biedermann [c], G. Cseh [a], G. Kocsis [a], M. Krause [c], T. Szepesi [a], M. Szűcs [a,1], The W7X Team [c,2]

[a] HUN-REN Centre for Energy Research, Institute for Atomic Energy Research, Konkoly-Thege Miklos rd 29-33., Budapest, 1121, Hungary
[b] Budapest University of Engineering and Economics, Institute of Nuclear Techniques, Department of Nuclear Techniques, Muegyetem rkp. 3., Budapest, 1111, Hungary
[c] Max Planck Institute for Plasma Physics, Wendelsteinstraße 1, Greifswald, 17491, Germany

ARTICLE INFO

Keywords:
Plasma size
Videodiagnostics
W7-X
Stellarator
Image processing

ABSTRACT

Determining the plasma size in the Wendelstein 7-X stellarator is complicated by the complex 3D structure and lack of axial symmetry. The effective radius (r_{eff}) of the visible radiation belt around the plasma gives a suitable estimate. This study presents a novel method to determine r_{eff} using the W7-X fast camera system. We correlate preprocessed EDICAM images with synthetic images based on the expected emissions of infinitesimally thin radiating layers from individual flux surfaces. Images are preprocessed to make the method reliable against wall reflections and increased divertor radiation. The width of the radiation belt is also estimated, which is relevant in the study of turbulent structures. We demonstrate the applications of this method in the case of detached and "breathing plasmas".

1. Introduction

The size of the plasma is one of its most apparent features. Its dynamics bear implications about the onset of detachment [1] or its power balance [2]. Yet, obvious as it may be, determining it in the case of W7-X may be less than straightforward due to the complex shape of the plasma.

Here, we measure plasma size by the size of the visible radiation belt observed by the W7-X Videodiagnostics system [3]. This radiation belt surrounds the plasma at the edge, where it is cool enough to shine in the visible range. It is a good indicator for estimating the size of plasmas, even with such complex shapes as those at the W7-X, by even a single camera image. This can be especially important for the commissioning of new devices to know whether the desired size and shape are successfully achieved. Knowing plasma size is also important during routine operations, as it is indicative of the power balance of the plasma. With a strong H puff, for example, the resulting edge radiation can induce the plasma to shrink to a fraction of its original size. Bolometry and Charge Exchange Spectroscopy confirmed that most of the emissions come from a few cm wide layer at the edge of these small plasmas [4]. According to a power balance model, an inverse relation can be given between the plasma density and its radius [4].

Change in plasma size also heralds the onset of detachment. At W7-X, in attached plasmas, most of the radiation originates from the divertor region [5]. During detachment, the radiation zone moves to the last closed flux surface (LCFS) [1,5], causing visible shrinkage.

Turbulent filaments are also visible in the radiation belt [6]. Its radial position and width are key for understanding the behavior of such filaments, providing further motivation for this research.

The rest of the paper is structured as follows: Section 2 gives the detail on the measurement setup and the applied methods, Section 3 shows examples of some practical applications, Section 4 summarizes the results and concludes this paper.

2. Measurement and methodology

The simplest way to describe the size of the plasma is by an effective radius (r_{eff}), which is the average small radius of a toroidal surface. This r_{eff} can be measured by the r_{eff} of the visible radiation belt at the plasma edge. Due to the complex magnetic geometry and lack

* Corresponding author at: HUN-REN Centre for Energy Research, Institute for Atomic Energy Research, Konkoly-Thege Miklos rd 29-33., Budapest, 1121, Hungary.
E-mail address: buzas.attila@ek.hun-ren.hu (A. Buzás).

[1] Present: Max Planck Institute for Plasma Physics, Boltzmannstrasse 2, Garching, 85748, Germany.
[2] See O. Grulke et al 2024 (https://doi.org/10.1088/1741-4326/ad2f4d).

https://doi.org/10.1016/j.fusengdes.2025.115304
Received 9 January 2025; Received in revised form 29 May 2025; Accepted 23 June 2025
Available online 8 July 2025

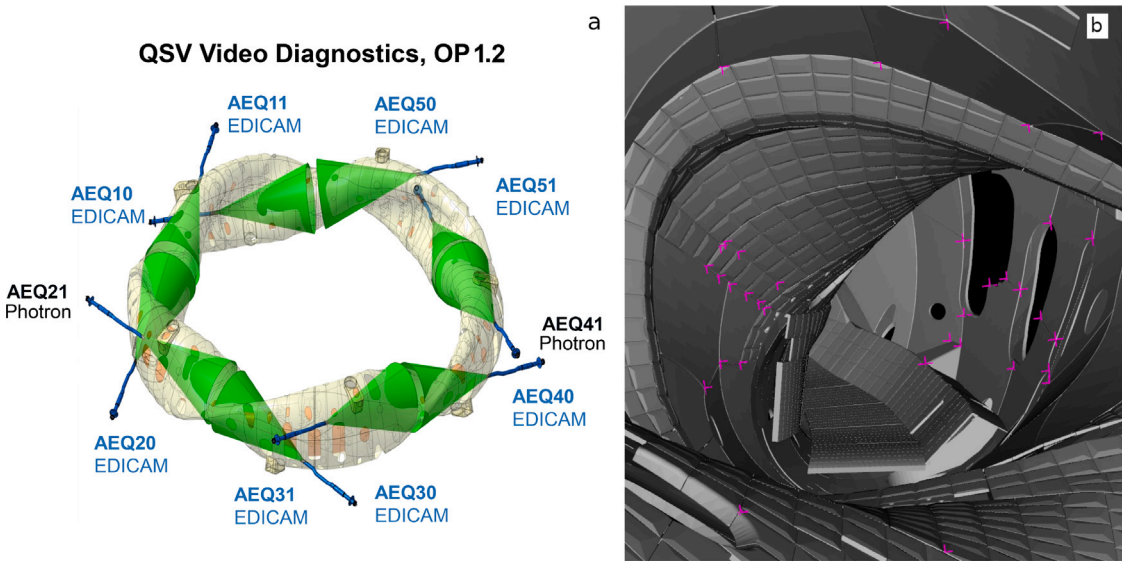

Fig. 1. (a) Schematics of the W7-X videodiagnostic system during OP1.2. The green cones field-of-views of the cameras. The two EDICAMs used for this study are marked. (b) CAD model view from AEQ31. This is what the camera would see without plasma. The pink crosses are the reference points used for spatial calibration.

of axial symmetry, estimating the size of the radiation belt is rather complicated. As the plasma twists and turns, parts of the image where the magnetic field lines are parallel with the line of sight (LoS) become brighter, and others dimmer. The resulting radiation pattern has a complex shape. It is also quite different from the cross-section of the flux surfaces at any given toroidal angle. The solution is to compare this pattern to synthetic camera images created from the reconstructed magnetic geometry of the plasma. This idea was first presented in [7]. It worked reasonably well in limiter configurations. However, with the introduction of the island divertors, a significant portion of the images become overexposed. Reflections, hotspots, transients, and other bright events caused by plasma-wall interactions (PWI) or manipulator probe plunges can cause a similar effect. The synthetic images overlapping with these bright patches score high and are flagged as a match mistakenly. It also gave no estimate for the width of the radiation belt. Here, we introduce several enhancements to make this a robust method. In the following subsections, we describe each step of the process in detail.

2.1. The W7-X videodiagnostics system

The best-suited diagnostic to observe the radiation belt is the W7-X videodiagnostics system. It consists of commercial Photron fast cameras and EDICAMs specifically designed for fusion experiments [8,9]. Fig. 1a shows the schematics of the videodiagnostic system during OP 1.2. Two EDICAMs observe each of the five segments of W7-X covering most of the plasma volume [10]. They tolerate magnetic fields up to 3T, have hardware support for multi-ROI (region-of-interest) event detection, and are capable of recording discharges with 1 Mp at 400 Hz (or up to 10 kHz with increasingly reduced ROI) [11,12]. Using the non-destructive read-out method, these ROIs can be recorded simultaneously with different framerates. For this analysis, the EDICAMs are more practical. During routine operations, the EDICAMs record the entire discharge with 100–200 Hz framerate (shots mentioned in this paper were recorded at 100 Hz). No optical filters are applied, and as they view the plasma from multiple angles, it is possible to compare results from different views at any moment. For this study, ports AEQ31 and AEQ50 were used. Fig. 1b shows what a camera would see without plasma by the CAD model view from port AEQ31. The camera itself is rotated 90 degrees to the left, which is why the actual images appear to be laying.

2.2. Constructing synthetic images

The synthetic images are created using the projections of the 3d reconstruction of W7-X flux surfaces. For the magnetic reconstruction, field line tracing was applied to the vacuum magnetic field. 3d coordinates from a given flux surface are projected to the view of a given camera (to demonstrate the projection, Fig. 2a shows field lines from the LCFS projected to an EDICAM image). The projected points over each pixel are summed up, producing an image representing the emission pattern of an infinitesimally thin, uniformly radiating layer at that flux surface (Fig. 2b shows an example belonging to the LCFS). The projection parameters are calculated from reference points of known 3d coordinates from the CAD model of the vacuum vessel (see Fig. 1). Each synthetic image is labeled by an r_{eff} value. It is the average small radius of the flux surface they are based on, defined as the radius of a circle with an area equal to the average cross-section of said flux surface in a segment of the device. Based on the precision of the magnetic reconstruction, the r_{eff} of the current set of synthetic images increases by 0.5–1.5 cm steps (mostly 0.5–1 cm). This defines the radial resolution of this method. The spatial resolution of the EDICAMs is around 1–2 mm, so further refinement is possible.

The construction of such images was first described in [13]. They work reliably enough, provided the radiation belt is inside the LCFS. However, the plasma often extends beyond that, so further refinement was necessary. For those cases, the gradually enlarged shape of the LCFS is used to create more synthetic images. The basis of this approach is the empirical observation that when the radiation belt is clearly outside the LCFS, its shape on the actual camera images is still very similar to its shape in the case of smaller plasmas. Visually comparing the best-matching enlarged image with the actual plasma shape shows reasonable agreement. As such, the estimate is deemed acceptable. With this method, a series of images is created with ca. 0.5 cm increments in r_{eff}, covering the entire volume of the vacuum vessel.

2.3. Reducing raw EDICAM images

While the outlines of the radiation belt are often quite pronounced on raw images, that is not always the case. To make the comparison between synthetic and EDICAM images more robust, we use a simple algorithm to find the parts of the images where the brightness increases

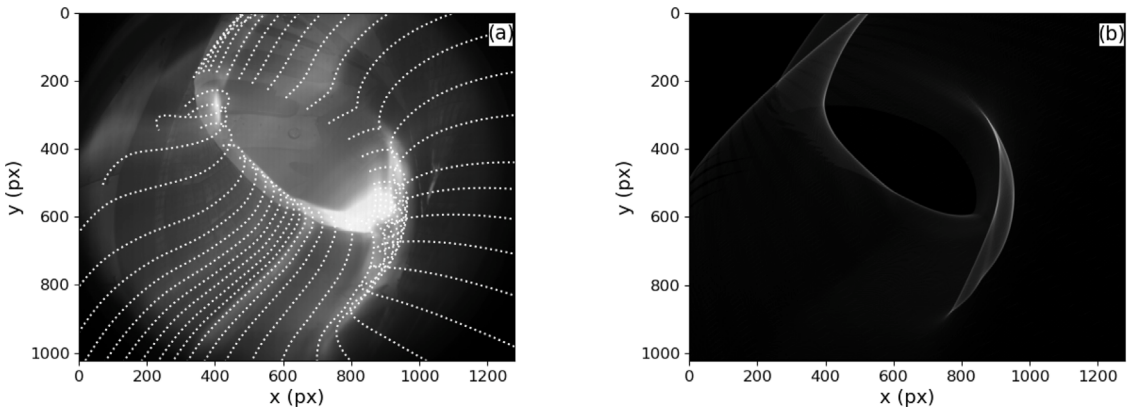

Fig. 2. (a) View of a detached plasma by the EDICAM from port AEQ31. Field lines from the LCFS are projected to represent the magnetic geometry. (b) Synthetic image based on the hypothetical radiation of the LCFS.

intensely. To make the transitions smoother and the results more distinct, first we smooth the raw images with a Gaussian window. A σ of 3 pixels for the window is quite sufficient. Then, we calculate the absolute value of the gradient of the image. The result is multiplied pixel-wise by the smoothed image. This serves to enhance the parts where the plasma becomes brighter and suppress the parts where the background changes brightness (at the diagnostic ports for example). This method highlights the pixels where strong change in intensity happens, such as the edges of the radiation belt. It is reasonably effective in the case of small plasmas, where the source of all the light is the radiation belt. However, it is still sensitive to the consequences of PWIs and transients, making it less effective in the case of fully extended plasmas (especially in the divertor region, which is usually overexposed). Examples of the overexposed divertor or bright filamentary structures are shown in Fig. 3a. To avoid such effects, the algorithm is only applied to predefined ROIs, where the outlines of the radiation belt are usually quite distinct. The rest of the image is zeroed out. The other advantage of applying ROIs is that it makes it possible to focus the search on the inside or the outside of the radiation belt. The outlines of the radiation belt closer to the center match synthetic images of smaller r_{eff}. In turn, the outlines closer to the edge match bigger ones. As a result, it becomes possible to estimate the width of the radiation belt by using different ROIs. The different ROIs used for these purposes are highlighted in Fig. 3a for the view AEQ50. As no two views are identical, they, of course, require their own sets of ROIs. The ROIs for AEQ31 look quite similar, with only minor adjustments.

Fig. 3b shows the result of the algorithm applied to the entire Fig. 3a without ROIs. The overexposed parts at the divertor distort the outline, while some other features are lost in contrast. Applying the ROIs highlighted in Fig. 3a avoids these problems. Fig. 3c shows the results of the algorithm applied to the ROIs focusing on the inner edge of the radiation belt (dashed boxes in Fig. 3a). The algorithm is applied to each relevant ROI, then the compound image of the results is correlated with the synthetic images. The key features become more pronounced this way, while the problematic parts are gone. The best-matching synthetic image is superimposed for visual reference. Fig. 3d is created in a similar fashion but with ROIs focusing on the outer edge of the radiation belt (solid boxes on Fig. 3a).

The selection of the ROIs is manual and based on experience. The best-suited regions are those where the plasma does not interact with the wall and the field lines are parallel with the line-of-sight. Such regions are easily identifiable visually and remain well-defined over various magnetic configurations. However, if significant variation is expected in plasma shape and size, the ROIs can be tailored to the specific scenario, just as different synthetic images are required for different magnetic configurations. The ROIs shown in Fig. 3a are suitable for divertor configurations. For small plasmas, slightly larger ROIs are used at the center of the image. It is not necessary to update them during the analysis of a single discharge, and they are usable for different discharges. However, if the need arose to update them during analysis, it would be easy enough to implement.

2.4. Matching synthetic images to reduced images

To find the best match, the Pearson correlation coefficients of the reduced image and the synthetic images are calculated. The r_{eff} of the highest-scoring image is chosen.

$$\varrho_{X,Y} = \frac{\mathbb{E}[(X-\mu_X)(Y-\mu_Y)]}{\sigma_X \sigma_Y} \tag{1}$$

Here, X and Y are the compared images, μ and σ are their means and standard deviations.

3. Results and applications

Since the radiation belt has a few cm radial width, estimating its position is somewhat arbitrary. Bolometry measurements found its width in the case of small plasmas to be about 5 cm [1]. This is consistent with assumptions based on the lifetime of plasma filaments observed with fast cameras [6]. Indeed, for studying turbulence, the width of the radiation belt is just as important as its position.

Multiple methods were tested to find the width of the radiation belt. Of all these, the most robust turned out to be to use different ROIs (see Fig. 3) to find its inner and outer edges. The mean of these two values can be given as an estimate for the plasma size (r_{eff}). This shows good agreement with results calculated from power balance equations in the case of small plasmas [4]. Fig. 4a demonstrates the method in action in the case of a standard configuration plasma. It shows how the correlation changes for the two sets of ROIs, focusing on the inside and outside of the radiation belt, in the function of the r_{eff} of the synthetic images. The peaks of the two curves indicate the beginning and the end of the radiation belt, their distance its width. Since the two sets of ROIs overlap and the inside of the radiation belt is much brighter than the outside, there are two peaks on the curve of the outside ROIs (green line on Fig. 4a), and occasionally the first one is higher. For this reason, it is safer to choose the last peak of the curve instead of the highest one. The results of the comparison with the raw image are also plotted with dashed lines. While the estimate it gives is quite similar, it does not have any distinctive feature by which the width of the radiation belt could be determined. The peak of the curve from the raw images is often quite flat, making its estimate ambiguous. Fig. 4b shows the time evolution of the estimates for the inside and outside of the radiation belt using the two cameras. They measure the inner edge quite consistently, however, their estimates for the outer edge differ by approximately 2 cm. Consequently, the estimates for the width also differ by as much between the two views, as shown by Fig. 4c. It varies between 6–7 cm

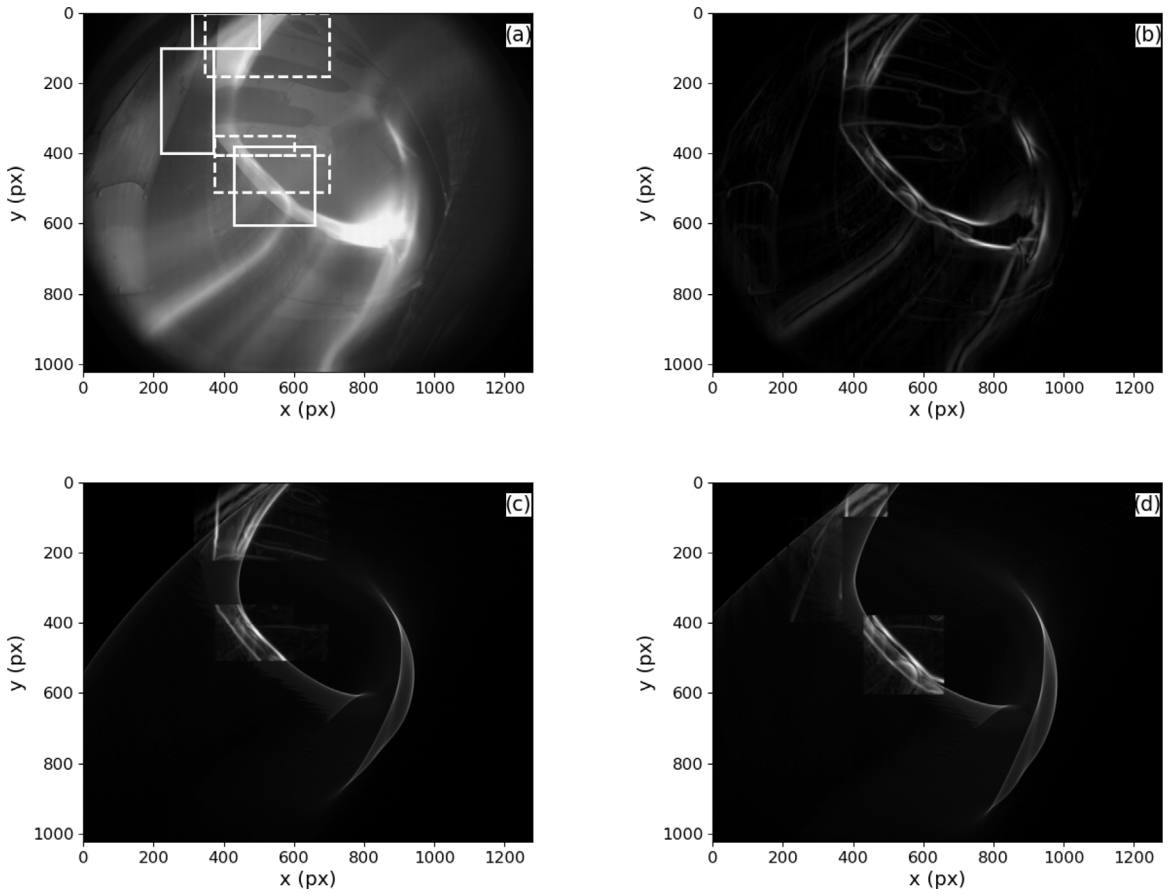

Fig. 3. (a) EDICAM image from port AEQ50 with different ROIs highlighted. ROIs for finding the inner edge of the radiation belt are plotted with dashed lines, ROIs for the outer edge with solid. (b) Result of the image reduction algorithm applied to the entire view. (c) Result of the algorithm applied to ROIs specific to the inner edge of the radiation belt with the matching synthetic image superimposed. (d) Result of the algorithm applied to ROIs specific to the outer edge of the radiation belt with the matching synthetic image.

for AEQ50 and 8–9 cm for AEQ31. Upon visual confirmation, both estimates seem accurate. The reason for this discrepancy is currently unknown. Uncovering why the thickness of the radiation belt changes between the two views requires further investigation, and as such, is out of the scope of the present paper. Fig. 4d shows the location of the radiation belt against the edge density profile to demonstrate that it is indeed a good indicator of the plasma size. The density profile is reconstructed by the alkali beam [14], the edges of the radiation belt are plotted in red. For their position, the radial coordinates of the reference surfaces, by which the synthetic images are made, are used along the path of the alkali beam. This is the reason why it appears narrower than in the previous figures. The position of the LCFS is added for reference.

Monitoring the plasma size during a discharge can yield insight into the state and power balance of the plasma. [5] shows that a significant portion of the visible radiations move radially inwards from the divertors during detachment. As such, a sudden, small drop in size may indicate the onset of detachment. Fig. 5a shows such a case in a standard configuration shot. Detachment is confirmed by the steep rise in the radiation fraction (f_{rad}). The estimate from the raw images is also added to showcase the enhancements to the method. Using only the raw images underestimates the plasma size during attachment and completely misses the change direction at the onset of detachment. Change in the width of the radiation belt may also be indicative of the transition, as the increase in Fig. 4c correlates with the onset of detachment. This phenomenon, however, has not yet been investigated in depth. For more information on using fast cameras to detect detachment, please refer to [15].

Generally, there is strong anti-correlation between the plasma size and f_{rad}. When radiation power surpasses the heating power, the plasma is expected to cool down and shrink. The power balance model in [4] gives a relation between the plasma density and its size. According to the model, for a given set of plasma parameters, a higher density results in a smaller plasma. In the case of the so-called "breathing plasmas", periodic gas inlets can create a cycle. The increased density causes increased radiation, which causes the plasma to shrink. However, as the plasma cools, radiation is also reduced. This allows the plasma to bounce back and grow once more. Fig. 5b shows how the plasma size and f_{rad} are modulated with gas fueling in a low-ι discharge. There is a slight delay between f_{rad} and r_{eff}, indicating hysteresis-like behavior. The analysis of the exact nature of this behavior is still ongoing.

4. Conclusions

In this paper, we introduced a novel method to estimate the plasma size for the W7-X stellarator. Estimations are based on the effective radius of the visible radiation belt at the edge of the plasma. This application can work with any kind of camera operating in the visible range. It currently uses the EDICAM cameras of the W7-X videodiagnostic system. Those cameras are especially suited for this purpose, as they view the entire poloidal cross-section in high resolution from multiple locations, and are highly adaptable to specific needs. Their non-destructive readout capability, allowing them to record parts of the view at higher framerates, could further enhance the method. This could be useful in studying the fast dynamics of the radiation belt for example.

The EDICAM images are reduced to find the regions where a huge increase in brightness occurs. This serves to emphasize the edges of the

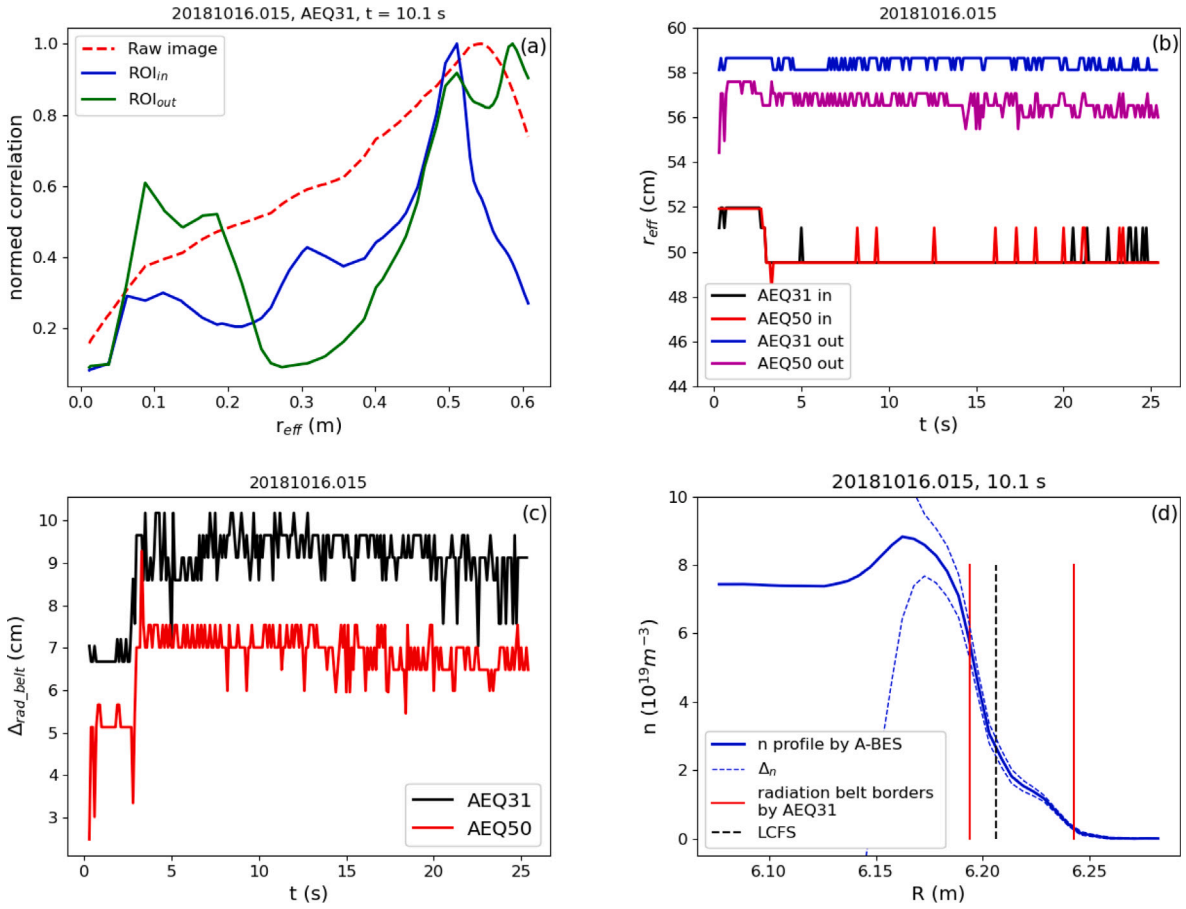

Fig. 4. The titles indicate the shot number, the view used for the measurement, and the time stamp (where applicable). (a) Scores of individual synthetic images against their r_{eff} using the two sets of ROIs and the raw image. The three curves are normed by their highest value to bring them to the same scale. (b) Time evolution of the estimates of the inner and outer edges of the radiation belt from two separate views. Sampled at 10 Hz. (c) Evolution of the width of the radiation belt during a discharge from separate views. Also sampled at 10 Hz. (d) Position of the radiation belt against the density profile (Δ_n is the uncertainty of the profile reconstruction). The position of the LCFS is highlighted by the black dashed line.

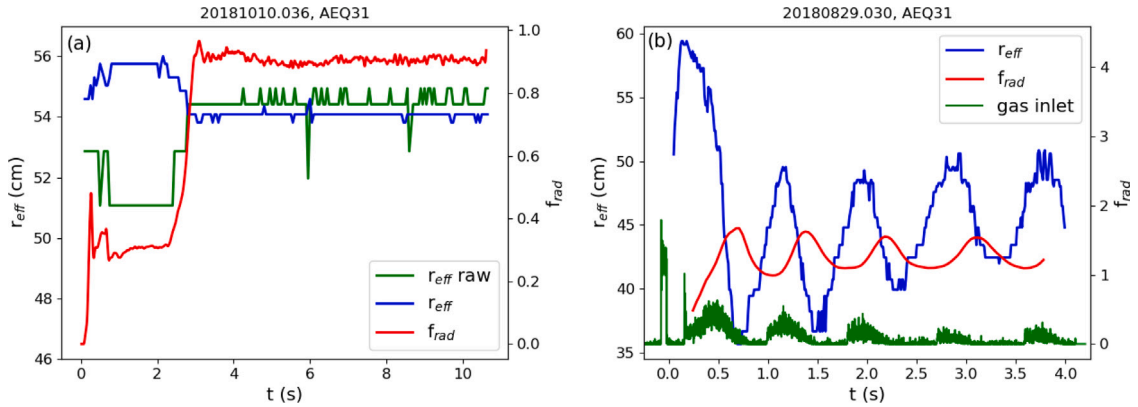

Fig. 5. (a) Evolution of the plasma size (mean of the r_{eff} of the inner and outer edges of the radiation belt) and f_{rad} against time in a standard configuration shot. The abrupt change indicates the onset of detachment. Results from the raw images are added for comparison. Sampled at 20 Hz. (b) Change of plasma size and f_{rad} after gas fueling during a "breathing plasma" in a low-ι discharge. Sampled at 100 Hz.

radiation belt. Applying this algorithm to specific ROIs increases the robustness of the method against effects caused by PWIs. The reduced images are correlated with synthetic images representing the hypothetical emissions of individual flux surfaces to find the best match. The final estimation is given by the effective radii of the best-matching images. This method also gives an estimation for the width of the radiation belt, which is consistent with expectations based on turbulence studies.

Finally, we demonstrate the usefulness of the method in various applications, such as the study of turbulent structures in the edge and the power balance of the plasma. Indeed, plotting the plasma size against the radiation fraction shows a strong dependence, which is particularly evident in the case of breathing plasmas or at the onset of detachment. These preliminary results may provide the basis for a wide range of future research.

CRediT authorship contribution statement

A. Buzás: Writing – review & editing, Writing – original draft, Visualization, Software, Methodology, Investigation, Conceptualization, Formal analysis. **C. Biedermann:** Resources, Data curation. **G. Cseh:** Investigation, Formal analysis, Data curation. **G. Kocsis:** Supervision, Resources, Data curation, Conceptualization. **M. Krause:** Resources, Data curation. **T. Szepesi:** Supervision, Resources, Project administration, Methodology, Data curation, Conceptualization. **M. Szűcs:** Methodology, Investigation, Formal analysis, Conceptualization.

Declaration of competing interest

The authors declare the following financial interests/personal relationships which may be considered as potential competing interests: Attila Buzas reports financial support was provided by European Consortium for the Development of Fusion Energy. Attila Buzas reports a relationship with European Consortium for the Development of Fusion Energy that includes: travel reimbursement. If there are other authors, they declare that they have no known competing financial interests or personal relationships that could have appeared to influence the work reported in this paper.

Acknowledgments

This work has been carried out within the framework of the EUROfusion Consortium, funded by the European Union via the Euratom Research and Training Programme (Grant Agreement No 101052200 — EUROfusion). Views and opinions expressed are however those of the author(s) only and do not necessarily reflect those of the European Union or the European Commission. Neither the European Union nor the European Commission can be held responsible for them.

Data availability

Data will be made available on request.

References

[1] Y. Feng, et al., Nucl. Fusion 61 (2021) 086012, http://dx.doi.org/10.1088/1741-4326/ac0772.
[2] K. Itoh, et al., J. Phys. Soc. Japan 57 (1988) 1269, http://dx.doi.org/10.1143/JPSJ.57.1269.
[3] G. Kocsis, et al., Fusion Eng. Des. 96–97 (2015) 808, http://dx.doi.org/10.1016/j.fusengdes.2015.02.067.
[4] A. Pandey, et al., 23rd International Stellarator and Heliotron Workshop, 2022, https://www.ifpilm.pl/images/ishw2021/Oral_presentations/Arun_Pandey.pdf.
[5] E. Wang, et al., Nucl. Mater. Energy 33 (2022) 101283, http://dx.doi.org/10.1016/j.nme.2022.101283.
[6] A. Buzas, et al., Nucl. Fusion 64 (2024) 066012, http://dx.doi.org/10.1088/1741-4326/ad365e.
[7] T. Szepesi, et al., 44th EPS Conf. on Plasma Phys. ECA, 41F, P5.119, 2017, https://info.fusion.ciemat.es/OCS/EPS2017PAP/pdf/P5.119.pdf.
[8] S. Zoletnik, et al., Fusion Eng. Des. 88 (2013) 1405, http://dx.doi.org/10.1016/j.fusengdes.2013.01.054.
[9] T. Szepesi, et al., Fusion Eng. Des. 153 (2020) 111505, http://dx.doi.org/10.1016/j.fusengdes.2020.111505.
[10] S. Zoletnik, et al., Rev. Sci. Instrum. 89 (2018) 013502, http://dx.doi.org/10.1063/1.4995947.
[11] T. Szabolics, et al., Fusion Eng. Des. 96–97 (2015) 980, http://dx.doi.org/10.1016/j.fusengdes.2015.03.040.
[12] T. Szepesi, et al., Fusion Eng. Des. 146 (2019) 874, http://dx.doi.org/10.1016/j.fusengdes.2019.01.103.
[13] T. Szepesi, et al., 43th EPS Conf. on Plasma Phys. ECA 40A, P4.004, 2016, https://info.fusion.ciemat.es/OCS/EPS2016PAP/pdf/P4.004.pdf.
[14] M. Vécsei, et al., Rev. Sci. Instrum. 92 (2021) 113501, http://dx.doi.org/10.1063/5.0057158.
[15] M. Szucs, et al., Mach. Learn. Appl. Sci. 12 (2022) 269, http://dx.doi.org/10.3390/app12010269.